Structuring and Functionalisation of Titania

A thesis presented in partial fulfillment of the requirements for the degree of

Doctor of Philosophy
in
Chemistry

at Massey University, Palmerston North, New Zealand.

Yvonne PeeYee TING

2008

ABSTRACT

Grätzel cells are liquid-electrolyte photoelectrochemical cells that contain dye-sensitised titania electrodes. The sensitiser is typically an organic species that absorbs visible light and increases the spectral region in which Grätzel cells may produce electricity. A key feature in the success of Grätzel cells is the high surface area of nanostructured titania electrodes. In this study, the nanostructuring of titania has been explored by two complementary methods: templation and self-assembly.

The templation of silica colloidal crystals (opals) was chosen as an inverse opal of titania would display a porous, bicontinuous structure in addition to a photonic band-gap. A diverse variety of titania inverse opals was produced, ranging from ideal 'honeycomb' to non-ideal 'grape-like' morphologies. However, the fragility of the material and difficulties in reproduction meant that the testing of such electrodes within Grätzel cells was limited.

Study towards the formation of a nanoparticle superlattice of titania via chemically-assisted self-assembly involved the investigation of both nanostructured titania surfaces and dye adsorption. The mode of dye binding to titania and the stability of adsorbed dyes was studied to aid work toward the design of a self-assembled titania superlattice, as well as to assist in the analysis of dye performance in Grätzel cells. Crystalline, aggregated titania and amorphous, dispersible titania was produced for dye binding studies of small organic carboxylic acid dyes. It was found that while dyes are adsorbed and intimately associated with titania, the mode of dye binding is different on a dry electrode than upon dispersed and solvated titania. The dyes appear to be bound to titania in a carboxylate form in the dry state, but in a mode that closer resembles that of the native dye upon dispersed titania.

ACKNOWLEDGEMENTS

I would like to thank all of the people who have helped me over the past four years and who have helped to make my doctoral experience a wonderful one. A tremendous "Thank you!" to David L. Officer and Mark R. Waterland for their supervision of my studies with great foresight and guidance!

Thanks also to the past and present members of the Nanomaterials Research Center (NRC) and the Institute of Fundamental Sciences at Massey University, all of who have been generous with their professional advice and time.

I would like to give a huge "Cheers!" to my husband David, my parents (Kooi Hong and Song Bong) and sisters (Valeska, Caroline & Edwina) for their support and confidence in my abilities – all without losing the plot! %:)

The support given by the MacDiarmid Institute for Advanced Materials and Nanotechnology in the form of my scholarship is also gratefully acknowledged.

Acknowlegments for technical help:

AFM and STM: Richard Havercamp, Anita Sharma and Aaron Marshall of the Institute of Technology and Engineering, Massey University for training.
Dynamic Light Scattering: Reza Mozafari of the Riddet Centre, Massey University for training.
Electron Microscopy: Douglas Hopcroft and Raymond Bennett of the Electron Micrography Suite, Massey University (ex-HortResearch) for collection of SEM images, energy dispersive X-ray analysis and for training on the TEM. David Flynn and Richard Tilley of the Electron Microscopy suite, Victoria University of Wellington for the acquisition of TEM and SEM images. Aaron Hicks of the Institute of Veterinary Animal and Biomedical Sciences, Massey University for training on the techniques of embedding and sectioning samples for TEM.

Nuclear Magnetic Resonance Spectroscopy: Patrick Edwards of the Institute of Fundamental Sciences, Massey University for collection of ^{1}H spin-echo and diffusion experiments.

Optical Microscopy: Elizabeth Nickless of the Institute of Molecular & Biological Sciences, Massey University, for training on the 100x Olympus microscope.

Profilometer: Andrea Bubendorfer of the Materials Physics Team, Industrial Research Limited for training and use of the equipment.

Raman Spectroscopy: Mark Waterland and Adam Swanson of the Institute of Fundamental Sciences, Massey University for training and help in using the apparatus. Geoff Waterhouse of the University of Auckland for the collection of backscattered resonance Raman spectra of titania films.

Solar Cell Testing: Wayne Campbell of the Nanomaterials Research Centre, Massey University for training on how to assemble and test dye-sensitised solar-cells.

Voltammetry: Klaudia Wagner of the Nanomaterials Research Centre, Massey University for training.

X-ray Diffraction: Gordon Heeley of the School of Physical and Chemical Sciences, Victoria University of Wellington and Robert Stewart of the Soil & Earth Sciences Group, Institute of Natural Resources, Massey University for training and use of the equipment. Tim Kemmit of the Materials Physics Team and Ian Brown of the Ceramics Team, Industrial Research Ltd for collection of grazing incidence XRD data.

For help with Chemistry and in the General Prevention of Insanity during the course of my doctoral studies: the past and present members of the NRC!

Amy Ballantyne, Warrick Belcher, Robert Breukers, Shannon Bullock, Wayne Campbell, Loretta Crowe, Beatrice Eccles, Sonja Ensink, Daina Grant, Sanjeev Ghambir, Sun Hao, Fabio Lodato, Donna Royal, Adam Stephenson, Mark Vigniswaran, Pawel & Klaudia Wagner, Amy Watson.

TABLE OF CONTENTS

Structuring and Functionalisation of Titania *i*

Abstract *iii*

Acknowledgments *iv*

Table of Contents *vii*

List of Tables, Figures and Equations *xi*

Abbreviations *xxii*

Definitions and Synonyms *xxiii*

Pictorial Tables of Organic Species *xxvi*

1. INTRODUCTION *1*

1.1. Titania *1*

1.2. Applications of Titania *3*

1.3. Solar Cells *4*
1.3.1. Fully Inorganic Devices *5*
1.3.2. Organic Heterojunction Devices *6*
1.3.3. The Grätzel Cell *8*
1.3.4. Titania for Grätzel Cells *11*

1.4. The Nanostructuring of Materials *12*
1.4.1. Templated Nanostructures *12*
1.4.2. Template-less Nanostructures *14*

1.5. The Nanostructuring of Titania *15*
1.5.1. Templated Nanostructures of Titania *16*
1.5.2. Inverse Opals of Titania *18*
1.5.3. Template-less Nanostructures of Titania *19*
1.5.4. Self-Assembly of Titania using Small Molecules *21*

1.6. Sensitiser Binding to Titania for Grätzel Cells *25*
1.6.1. The Binding of Dye to Titania *26*

1.7. Opportunities for Novel Research in Nanostructured and Functionalised Titania *29*

1.8. Objectives and Hypotheses *30*

1.9. References *31*

2. *SYNTHESES OF TITANIA, MOLECULES FOR ITS SELF-ASSEMBLY, DYEING AND EXPERIMENTAL TECHNIQUES* 43

2.1. *Materials* 43

2.2. *Techniques* 43

2.3. *Nanostructured Titania: Inverse Opals* 48
- 2.3.1. *Colloid Synthesis* 48
- 2.3.2. *Opal Formation* 48
- 2.3.3. *Inverse Opals of Titania* 49

2.4. *Nanostructured Titania for Binding Studies* 50
- 2.4.1. *Thin and Non-porous Titania* 50
- 2.4.2. *Aggregated and Sintered Titania* 51
- 2.4.3. *Dispersible Titania* 52

2.5. *Towards the Self-Assembly of Titania using Small Molecules* 52
- 2.5.1 *The Functionalisation of ITO Electrodes* 54
- 2.5.2. *Towards Chemically-Assisted Self-Assembled Titania Arrays* 58

2.6. *The Binding of Dye to Titania* 58
- 2.6.1. *UV-Vis Spectroscopy* 59
- 2.6.2. *FTIR Spectroscopy* 59
- 2.6.3. *Raman and Fluorescence Spectroscopy* 60
- 2.6.4. *NMR Spectroscopy* 60

2.7. *Solar Cell Testing* 61

2.8. *References* 64

3. *NANOSTRUCTURED TITANIA: INVERSE OPALS* 67

3.1. *Introduction* 67

3.2. *Opals* 68

3.3. *Inverse Opals* 69

3.4. *Opaline Templates of Silica* 70

3.5. *Titania Inverse Opals* 73

3.6. *Conclusions* 85

3.7. *References* 87

4. *NANOSTRUCTURED TITANIA FOR BINDING STUDIES* 91

4.1. *Introduction* 91

4.2. *Thin and Non-porous Titania* 92

4.3. *Aggregated and Sintered Titania* 95

4.4. Dispersible Titania 100

4.5. Conclusions 102

4.6. References 104

5. TOWARDS THE SELF-ASSEMBLY OF TITANIA USING SMALL MOLECULES 109

5.1. Introduction 109

5.2. Surface Functionalisation and Particle Binding 110

5.3. The Functionalisation of ITO Electrodes 113

5.4. The Binding of Amines and Carboxylic Acids to ITO 116

5.5. The Adsorption of Small Aromatic Molecules 119

5.6. The Adsorption of Ferrocene Derivatives 125
5.6.1. UV-Vis Spectroscopy 125
5.6.2. Voltammetry 130
5.6.3. Surface Coverage Estimates 139

5.7. Towards Chemically-Assisted Self-Assembled Titania Arrays 140

5.8. Conclusions 141

5.9. References 143

6. THE BINDING OF DYE TO TITANIA 149

6.1. Introduction 149

6.2. Dye Adsorption on Titania for Grätzel Cells 149
6.2.1. The Binding of Carboxylic Acids to Titania 150

6.3 Dye Aggregation, Solvent and Concentration Effects 152

6.4. Carboxylic Acid Probe Dyes 156

6.5. Spectroscopic Analysis of Adsorbed Dyes & Dye Adsorption 157
6.5.1. UV-Vis Spectroscopy 163
6.5.1.1. Dye Loading on Titania 163
6.5.1.2. Aggregation Studies 166
6.5.1.2.1. Introduction 166
6.5.1.2.2. Overview of UV-Vis Signal Shifts 167
6.5.1.2.3. Probe Dyes on Sol-Gel Titania 168
6.5.1.2.4. Probe Dyes on Dyesol Titania 169
6.5.1.2.5. Solvent Effects 171
6.5.1.2.6. Support for Equilibrium Dye Binding 173
6.5.1.2.7. Impact of Structure on Dye Aggregation 175
6.5.1.2.8. Aggregation of Porphyrinic Dyes 184
6.5.1.2.9. Summary 189

6.5.3. FTIR Spectroscopy *189*
6.5.3.1. Introduction *189*
6.5.3.2. Computer Modelling and Experimental Results *190*
6.5.3.3. Summary *205*

6.5.4. Raman and Fluorescence Spectroscopy *205*
6.5.4.1. Experimental Results *205*
6.5.4.2. Summary *209*

6.5.5. NMR Spectroscopy *210*
6.5.5.1. Introduction *210*
6.5.5.2. Preliminary Experiments *211*
*6.5.5.3. Adsorption of Dye **6.1** on Sol-Gel Titania* *218*
6.5.5.4. Summary *228*

6.6. Section Summary *229*

6.7. References *231*

7. CONCLUSIONS *237*

7.1. Overview *237*

7.2. Key Findings *237*

7.3. Discussion *239*

7.4. Future Directions *241*

7.5. References *243*

8. SUPPLEMENTARY DATA *245*

8.1. Chapter 4 *245*

8.2. Chapter 6 *245*

LIST OF TABLES, FIGURES AND EQUATIONS

Section 1.1.

Table 1.1. Physical properties of the low-temperature titania polymorphs.

Figure 1.1. Representations of the crystal unit cells for rutile, anatase and brookite.

Figure 1.2. Phase diagram for anatase and rutile and two alternative forms of titania. Data from three different sources are plotted.

Section 1.2.

Equation 1.1. The tilanol and tiloxane equilibrium.

Section 1.3.1.

Figure 1.3. Schematic of a multi-junction, tandem GaAs/$GaInP_2$ solar cell, as described by S. K. Deb, 1998.

Section 1.3.2.

Figure 1.4. Cartoon of a solar cell using MEH-PPV and buckminsterfullerene. The associated energy level diagram is shown, as described by A. Moliton, 2004.

Section 1.3.3.

Figure 1.5. Chlorophyll a.

Figure 1.6. Cartoon of a Grätzel cell with the associated energy level diagram for an anatase titania electrode sensitised by dye WMC-299b, 4-(2'-(5',10',15',20'-tetraxylylporphyrinatozinc(II)yl)butadienylmalonic acid, an iodine/triiodide electrolyte and a platinum counter electrode. 'CB' is the conduction band energy of titania, 'I_3^-/I^-' is the energy level of the iodide/triiodide couple.

Section 1.4.1.

Figure 1.7. A cartoon representation of a binary opal composed of large polystyrene spheres and smaller silica spheres (a) and the resulting array of sintered silica spheres (b).

Section 1.5.1.

Figure 1.8. A representation of the patterning of titania upon gold via the sacrificial organic intermediary of polystyrene.

Section 1.5.2.

Figure 1.9. A cartoon of a binary opal (a) and the resulting inverse opal (b).

Section 1.5.4.

Figure 1.10. Potential strategies for forming the first particulate layer of a titania array upon indium-doped tin oxide (ITO). a) A diacid linker binding titania directly to ITO. b) Pre-treatment of ITO with a diamine with binding of acid-functionalised titania via salt-formation. c) Pre-treatment of ITO with an amphiprotic linker and binding of pre-sensitised titania without an intervening salt layer.

Figure 1.11. A schematic of the porphyrin dyad assembly studied by Y.-J Cho *et al*. 2005.
Figure 1.12. A schematic of the 'quaternary structure' studied by H. Imahori *et al*. 2004.

Section 1.6.
Figure 1.13. a) The "green" zinc porphyrin dye, 2-cyano-3-(2'-(5',10',15',20'-tetraphenylporphyrinato zinc(II)yl)acrylic acid. b) The ruthenium "N3" dye, di(thiocyanato)-bis(2,2'-bipyridyl-4,4'-dicarboxylate) ruthenate(II) di-anion. c) The "Black" dye, tri(thiocyanato)-2,2',2"-terpyridyl-4,4',4"-tricarboxylate ruthenate(II) di-anion.

Section 1.6.1.
Figure 1.14. Ru(II)LL'CN. L is 4'-phosphonic acid-2,2':6'2''-terpyridine and L' is 1,2-bis(4'-methyl-2,2'-bipyridyl-4-yl)ethane.

Section 2.5.1.
Figure 2.1. Chem3D® representations of 5.4 with estimates of the maximum and minimum rectangular footprint area. For clarity, only one cyclopentadiene ring of the ferrocenyl group is shown.

Section 2.7.
Figure 2.2. A sample holder containing a DSSC with a green porphyrin dye on a nanocrystalline, mesoporous titania electrode.

Section 3.1.
Figure 3.1. A schematic of the concept of Bragg diffraction of light from a regular, periodic array.

Section 3.4.
Figure 3.2. SEM image of a silica opal deposited upon glass. The scale bar is for 1 μm.
Figure 3.3. a) The opal composed of 250 nm silica spheres displays the Bragg diffraction of green light, while the opal made of 350 nm spheres diffracts orange light. b) Detail of silica colloids, with titania nanocrystals. Square and hexagonal close-packing is highlighted. The scale bar is for 100 nm.
Figure 3.4. a) A typical, fractured silica opal. b) The same opal at a higher magnification. The scale bars are for 1 μm.

Section 3.5.
Figure 3.5. a) An inverse opal that resembles sealed 'honeycomb'. b) An inverse opal exhibiting a 'grape'-like morphology. The scale bars are for 100 nm.
Figure 3.6. a) The desired 'honeycomb' morphology. Note that windows connect adjacent air-spheres and that the interstices appear to be completely filled. b) Partial, almost 'skeletal' inverse opals. The scale bars are for 100 nm.
Figure 3.7. a) Granular and fibrillar titania nanoparticles may be observed on lightly-templated silica colloids, particularly where colloids meet. b)

Titania inverse opal formed by six cycles of infiltration and rinsing, with two treatments with water, then sintered at 500ºC. c) An inverse opal displaying a 'coral'-like morphology was displayed, perhaps due to sintering. The sample was treated twice with: three cycles of infiltration and rinsing, a treatment with water and sintering at 500ºC. Both samples used 1 : 40 : 0.6 infiltrate and 1 : 120 : 0.6 rinsing solutions. The scale bars are for 100 nm.

Table 3.1. The typical treatment protocol to form inverse opals of titania.

Figure 3.8. a) Disordered, fragmented material from a sample that was not treated with water. b) Condensed matter that resulted from two cycles of infiltration and rinsing, without treatment with water. The scale bars are for 1 μm.

Figure 3.9. a) TEM image of a cross-section of a titania inverse opal, illustrating open fractures and a sealed top-face. The scale bar is for 200 μm. b) SEM image of sample which was treated with rinsing steps. Colloids at the crack faces were cleanly templated, without excess titania occupying the crevice. The scale bar is for 100 nm.

Figure 3.10. a) Titania film contracted away from the inverse opal below. This sample had six infiltrations and a treatment with water. The scale bar is for 1 μm. b) The 'honeycomb' morphology, which is composed of thin titania shells. This sample was infiltered five times and treated once with water. The scale bar is for 100 nm.

Figure 3.11. These samples used an infiltrate with a mole ratio of 1 : 20 : 0.6 and a rinsing solution with 1 : 80 : 0.6 of titanium isopropoxide to dry ethanol to diethanol amine. The scale bar is for 1 μm. a) A 'basement' layer of inverse opal that exhibited practically no shrinkage. The opal had two cycles of infiltration, rinsing and treatment with water. b) Significant warpage and shrinkage was observed for this sample that was infiltered six times and air-dried, before sintering. The scale bar is for 100 nm.

Figure 3.12. a) Titania-silica composite formed by six cycles of infiltration and rinsing, with two treatments with water, then sintered at 500ºC. Mole ratios of 1 : 40 : 0.6 and 1 : 120 : 0.6 for reactants were used for infiltration and rinsing, respectively. The scale bar is for 100 nm. b) The resulting inverse opal displays a 'grape-like' morphology. The scale bar is for 1 μm.

Figure 3.13. a) Inverse opaline titania, with long-range structure. Twelve cycles of infiltration with centrifugation, then rinsing was followed by one treatment with water before sintering at 500ºC. Mole ratios of 1 : 40 : 0.6 and 1 : 120 : 0.6 for reactants were used for the infiltration and rinsing solutions, respectively. The scale bar is for 1 μm. b) A structure that resembles 'grapes'. Six cycles of infiltration were followed with two treatments with water. Solutions with mole ratios of 1 : 20 : 0.6 for both the infiltrate and rinsing solutions were used. The scale bar is for 100 nm.

Figure 3.14. The difficulty of obtaining reproducible inverse opals is illustrated. Both of these samples were treated by twelve cycles of infiltration with centrifugation and rinsing. This was followed by one treatment with water before sintering at 500ºC. Molar ratios of 1 : 40 : 0.6 and 1 : 120 : 0.6 for reactants were used for the infiltration and rinsing

solutions, respectively. a) The desired 'honeycomb' structure is displayed with filled interstices and windows to adjacent air-spheres. Fractures such as these were common. The scale bar is for 1 µm. b) Open-face 'honeycomb' material was received, but with extensive cracking and large variation in film thickness. The scale bar is for 10 µm.

Section 4.2.

Figure 4.1. a) A SEM image of flat and dense titania with two coats. b) A contact mode AFM image of thin and non-porous titania formed by two sequential dip-coats into a solution of with a 1 : 40 : 0.6 molar ratio of titanium isopropoxide : dry ethanol : diethanolamine. A 40 mm min^{-1} dip speed was used to produce a film with a RMS roughness of 10 nm.

Figure 4.2. Cyclic voltammetry of blank ITO and ITO dip-coated with thin and non-porous titania in a 1 mM hexacyanoferrate solution. Redox activity is suppressed with increasing coats of thin and non-porous titania. Voltage is given with respect to a $Ag/AgNO_3$ psuedo-reference electrode. The electrolyte was 0.1 M tetrabutylammonium perchlorate in acetonitrile. The scan rate was 100 mV s^{-1}.

Section 4.3.

Figure 4.3. a) Dyesol opaque titania plate, 12 µm thick. b) Screen-printed Dyesol transparent paste, 4 µm thick. c) Screen-printed Degussa P25, 4 µm thick. d) Spin-thinned sol-gel titania, 1 µm thick.

Figure 4.4. a) Titania of the Dyesol screen-printing paste for transparent films. b) Degussa P25 hydrophillic fumed titania. c) Sintered sol-gel titania.

Section 5.2.

Figure 5.1. A cartoon of the base unit of the composite material described by R. Frantz *et al*. 2004.

Figure 5.2. A dye used in the sol-gel preparation of a composite material for testing within Grätzel cells, as described by C. L. Lin *et al*. 2006.

Section 5.3.

Figure 5.3. Di(3-aminopropyl)viologen, as described by K. H. Hyung, 2003.

Figure 5.4. 4,4'-bis(*N*-napth-1-yl-*N*-phenylamine)-1,1'-biphenyl, as described by Q. T. Lee *et al*. 2000.

Section 5.4.

Figure 5.5. a) 1,4-benzenedicarboxylic acid. b) 2,6-napthalenedicarboxylic acid.

Figure 5.6 The coordination compound of 4-(*trans*-2-(4-pyridinyl)ethenyl)benzoic acid and carbonyl(5',10',15',20'-tetraphenylporphyrinatoruthenium(II).

Figure 5.7. In order to receive useful UV-Vis spectra, it is essential to subtract the blank (reference) spectrum of the same piece of ITO glass as used for each adsorption experiment. The spectrum of piece 1, after subtraction of an earlier scan of the same piece of ITO produces the expected, featureless resultant. However, the spectrum of piece 1, after subtraction of a scan of a different piece of ITO creates an artificial result.

Section 5.5.
Table 5.1. UV-Vis absorption of aromatic species used in absorption studies.
Figure 5.8. UV-Vis spectra of ITO glass with drop-dried: 4-nitroaniline, 4-phenylenediamine.
Figure 5.9. UV-Vis spectra of species adsorbed onto ITO glass from 1 mM solutions in 1,4-dioxane: 4-phenylenediamine, 4-nitroaniline and 4-aminobenzoic acid. Glass absorbs below 300 nm, which produces a marked effect in subtracted spectra.
Figure 5.10. UV-Vis absorption for fresh 1,4-dioxane and for 1,4-dioxane heated at 80°C for two days.
Figure 5.11. UV-Vis solution spectra of 4-phenylenediamine kept within 1,4-dioxane, at 80°C. Shown are spectra corresponding to the initial solution and the solution after 21 hours and 4 days.
Table 5.2. UV-Vis absorbance peaks for polymeric material related to the probe species.

Section 5.6.1.
Table 5.3. UV-Vis absorption of solution spectra of ferrocene derivatives.
Figure 5.12. The effect of solvent on the deposition of 5.3 onto ITO glass: 1,4-dioxane, acetonitrile.
Figure 5.13. UV-Vis spectra of the imine 5.3 in methanol, drop-dried upon ITO glass and ITO glass treated by immersion from a 2 mM solution in 2,2-dimethoxypropane.
Figure 5.14. UV-Vis absorption spectra of ITO glass treated with 4-phenylenediamine, then with 5.2 to yield the overgrafted sample.
Figure 5.15. UV-Vis spectra of 5.4 in solution, drop-dried upon ITO glass and ITO glass treated by immersion from a 2 mM solution.
Figure 5.16. UV-Vis spectra of ITO glass treated by immersion within a 10 mM solution of 5.4 and a 5 mM solution of 5.1.

Section 5.6.2.
Figure 5.17. Cyclic voltammetry of within ITO glass was treated by immersion for an hour within a 2.5 mM solution in a 6% v/v solution of dry ethanol in hexane of either 5.1 or ferrocene. The sample was rinsed in a 5% v/v solution of 1,4-dioxane in hexane prior to voltammetry. The scans were done at 50 mV s^{-1} in acetonitrile.
Figure 5.18. The diffusion or degradation of adsorbed 5.1 off ITO glass over sequential cyclic voltammetry scans. The scans were done at 50 mV s^{-1} in acetonitrile.
Figure 5.19. Voltammetric plots of 5.3 in solution and adsorbed onto ITO glass. The scans were done at 100 mV s^{-1} in acetonitrile.
Figure 5.20. Cyclic voltammetry showing 5.3 deposited onto ITO glass by immersion within a 0.1 mM solution in 1,4-dioxane, at 85ºC for three days. The scans were done at 50 mV s^{-1} in acetonitrile.
Figure 5.21. Cyclic voltammetry showing the irreversible oxidation of 5.4 from a 10 mM solution results in a contamination of the electrode, as evidenced by the decreased current. The scans were done at 50 mV s^{-1} in acetonitrile.
Figure 5.22. Cyclic voltammetry scans of a 10 mM solution of 5.4. The half-wave potential for the reversible ferrocene/ferrocenium redox couple is

0.196 V_{SCE}. The scans were done at 50 mV s^{-1} in acetonitrile.
Figure 5.23. Cyclic voltammetry of 5.4 adsorbed upon ITO glass by immersion within a 2.3 mM solution, using 6% v/v 1,4-dioxane in hexane as the solvent. The scans were done at 50 mV s^{-1} in acetonitrile.
Figure 5.24. a) An ethenylferrocene and b) an ethynylferrocene, where 'Ar' represents aryl functionality, as described by L. Cuffe *et al*. 2005.
Figure 5.25. 2-ferrocenylmethylidenimino-5-methyl-benzoic acid (a) and 2-ferrocenylmethylamino-5-methylbenzoic acid (b), as described by J. Cano *et al*. 1995.

Section 5.6.3.
Figure 5.26. a) Bare ITO glass cleaned by washing with detergent, then ultrasonication within acetone, water, then ethanol. b) ITO glass treated with 4-aminobenzoic acid and Degussa P25 titania. A central area was swept clear of titania nanoparticles by the force of contact mode AFM.

Section 6.2.1.
Figure 6.1. Plausible binding modes of an adsorbate via carboxylic acid functionality to titania. Monodentate forms: a) pseudo-ester; b) carboxylate; c) bridging carboxylate. Bidentate forms: d) chelating; e) bridging; f) chelating and bridging.

Section 6.3.
Figure 6.2. A cartoon of a) H-aggregation and b) J-aggregation of di(thienylenevinylene)thiophene.
Figure 6.3. The origin of blue and red shifts in absorption on the formation of H- and J-aggregates as described by Mishra *et al*. 2000. The interaction between the electronic transition dipole moments of associated molecules results in additional excited states. Only one of the excited states is permitted, which for H-aggregates is that of higher energy and for J-aggregates is of lower energy.
Figure 6.4. Coumarin dyes as described by Z. S. Wang *et al*. 2005. a) Cyano(5,5-dimethyl-3-[2-(1,1,6,6-tetramethyl-10-oxo-2,3,5,6-tetrahydro-1*H*,4*H*,10*H*-11-oxa-3a-aza-benzo[de]anthracen-9-yl)vinyl]cyclohex-2-enylidene)acetic acid which bears a side ring on the alkene chain, which prevents aggregation. b) The analogous material, which is without a side ring and forms H-aggregates.
Figure 6.5. Hemin, the Fe^{3+} analogue of heme.
Figure 6.6. Glutamic acid as described by A. D. Roddick-Lanzilotta *et al*. 2000. Glutamic acid bound to titania by a) a single acid group and b) both acid functionalities.

Section 6.4.
Table 6.1. Spectral properties of carboxylic acid probe dyes.

Section 6.5
Figure 6.7. Chem3D® representations of 6.1 to 6.6 with estimates of the rectangular footprint area for dyes bound by only one carboxylic group.

Figure 6.8. Chem3D® representations of 6.1 to 6.6 with estimates of the rectangular footprint area for bound dye with potential binding groups towards the surface.
Table 6.2. Surface area of titania from nitrogen sorption data, unless otherwise stated.
Table 6.3. Range of the rectangular footprint areas of probe dyes (Figs 6.7, 6.8) and monolayer coverage values for dye upon sintered transparent Dyesol titania and native sol-gel titania.

Section 6.5.1.1.
Figure 6.9. UV-Vis absorbance over time for the 410 nm peak of 6.3 adsorbed onto sintered Dyesol titania plates from a 2 mM solution in tetrahydrofuran. The x-axis error bars are for ± 1 minute, the y-axis error bars are for ± 0.001 absorbance units.
Figure 6.10. Adsorption of 6.2 onto sintered Dyesol titania powder from a 2.3 mM methanolic solution and desorption in dry methanol. Data was collected for the UV-Vis maximum at 330 nm, the error bars are for conservative values of a ± 10% uncertainty for the calculated number of moles of 6.2 and ± 2 minutes of time. Similar data was obtained for 6.1.

Section 6.5.1.2.
Table 6.4. FWHM values for UV-Vis absorption signals of the probe dyes in tetrahydrofuran (THF) and on both dispersed sol-gel and sintered Dyesol titania.
Table 6.5. UV-Vis absorption of pure dyes in THF and on both dispersed sol-gel and sintered Dyesol titania.
Figure 6.11. UV-Vis spectra of a 1 : 1 and a 2 : 1 molar ratio of tetra-*n*-butylammonium hydroxide to 6.1 in methanol.
Table 6.6. UV-Vis absorption of pure dyes and dyed titania in solvent A.
Figure 6.12. UV-Vis spectra of 6.5 in tetrahydrofuran in a 1 : 5 v/v solution of tetrahydrofuran to 95% ethanol and adsorbed onto sintered titania plates.
Figure 6.13. A red shift of UV-Vis absorbance is observed when a titania plate dyed with 6.5 is wet with tetrahydrofuran is dried. The effect is reproducible as shown by further immersion of the plate in a solution of 6.5 and subsequent drying. The spectra are not subtracted for the titania blank in order to show that the wet plate is more transparent than the dry plate.
Figure 6.14. UV-Vis spectra of 6.4 in methanol, tetrahydrofuran, in a 1 : 5 v/v solution of tetrahydrofuran to 95% ethanol (solvent A) and with sol-gel titania in methanol, tetrahydrofuran and solvent A.
Equation 6.1. Equilibrium dye binding involving free and bound dye, only.
Equation 6.2. Equilibrium dye binding involving the available binding sites of titania and both free and bound dye.
Figure 6.15. UV-Vis spectra of 6.4, showing an absence of signal shoulders on titration with sol-gel titania in ethanol. Pure dye, a 339 : 1, a 21 : 1, and a 1 : 1 mole ratio of dye to titania. The FWHM values are 99 nm, 109 nm, 114 nm and 113 nm, respectively, with an uncertainty of 3%.
Figure 6.16. UV-Vis spectra of 6.1 in tetrahydrofuran, in acidic solution, in

solution with acidic-sol-gel titania. The mole ratio of sol-gel titania spheres 2 nm in diameter to dye was 1 : 5.
Figure 6.17. UV-Vis spectra of 6.2 in tetrahydrofuran, in acidic solution, in solution with acidic-sol-gel titania. The mole ratio of sol-gel titania spheres 2 nm in diameter to dye was 1 : 4.
Figure 6.18. UV-Vis spectra of 6.3 in tetrahydrofuran, in acidic solution, in solution with acidic-sol-gel titania and adsorbed onto sintered titania plates. The mole ratio of sol-gel titania spheres 2 nm in diameter to dye was 4 : 1.
Figure 6.19. UV-Vis spectra of 6.4 in tetrahydrofuran, in acidic solution, in solution with acidic-sol-gel titania and adsorbed on sintered titania plates. The mole ratio of sol-gel titania spheres 2 nm in diameter to dye was 4 : 1.
Figure 6.20. UV-Vis spectra of terthienylcyanoacrylic acid in tetrahydrofuran, in acidic solution, in solution with acidic-sol-gel titania and adsorbed on sintered titania plates. n(sol-gel titania spheres 2 nm in diameter) : n(dye) of 3 : 1.
Figure 6.21. UV-Vis spectra of terthienylvinylenemalonic acid in tetrahydrofuran, in acidic solution, in solution with acidic-sol-gel titania and adsorbed on sintered titania plates. n(sol-gel titania 2 nm in diameter) : n(dye) of 3 : 1.
Figure 6.22. A cartoon of possible aggregation and packing of a) 6.4 and b) 6.3 upon titania.
Figure 6.23. A depiction of the packing of a malonic acid with the binding groups a) parallel and b) staggered with respect to each other. The carbon atom labelled 'R' denotes the rest of the molecule.
Figure 6.24. UV-Vis spectra of 6.6 in tetrahydrofuran (507 nm), in acidic solution (514 nm), in solution with acidic-sol-gel titania (522 nm) and adsorbed onto sintered titania plates (510 nm). The mole ratio of sol-gel titania spheres 2 nm in diameter to dye was 4 : 1.
Figure 6.25. UV-Vis spectra of 6.5 in tetrahydrofuran, in acidic solution, in solution with acidic-sol-gel titania and adsorbed onto sintered titania plates. The mole ratio of sol-gel titania spheres 2 nm in diameter to dye was 4 : 1.
Figure 6.26. An extreme conformation of 6.6, where the ter(thienylenevinylene) group lies parallel to the surface.
Table 6.7. Porphyrin-based dyes used in dye aggregation studies.
Figure 6.27. UV-Vis spectra of sintered Dyesol titania dyed with 6.7 from a 0.2 mM solution in tetrahydrofuran. The dye absorbance increases with progressive immersion times of 2 min, 4 min, 12 min and 99 min.
Figure 6.28. UV-Vis spectra of sintered Dyesol titania dyed with 6.9 from a 0.2 mM solution in tetrahydrofuran. The dye absorbance increases with progressive immersion times of 2 min, 4 min, 8 min and 50 min.
Figure 6.29. UV-Vis spectra of sintered Dyesol titania dyed with 6.11 from a 0.2 mM solution in tetrahydrofuran. The dye absorbance increases with progressive immersion times of 2 min, 4 min, 10 min and 60 min.
Figure 6.30. UV-Vis spectra of sintered Dyesol titania dyed with 6.8 from a 0.2 mM solution in tetrahydrofuran. The dye absorbance increases with progressive immersion times of 2 min, 4 min, 13 min and 90 min.
Figure 6.31. UV-Vis spectra of sintered Dyesol titania dyed with 6.10 from a 0.2

mM solution in tetrahydrofuran. The dye absorbance increases with progressive immersion times of 2 min, 4 min, 12 min and 99 min.

Section 6.5.3.

Figure 6.32. ATR-FTIR spectra of native sol-gel titania and a sintered Dyesol titania plate. The fine structure in the spectra at 3700 and 1606 cm^{-1} are due to residual water.

Figure 6.33. Illustration of the two configurations (a) and (b) of 6.2 that were modelled for *ab initio* calculations.

Figure 6.34. Calculated vibrational data for configuration (a) of 6.2.

Figure 6.35. Calculated vibrational data for configuration (b) of 6.2.

Figure 6.36. Calculated vibrational data for configuration (c) of 6.2.

Figure 6.37. Calculated FTIR spectra for configuration (a) of 6.2 *in vacuo.*

Figure 6.38. Calculated FTIR spectra for configuration (b) of 6.2 *in vacuo.*

Figure 6.39. Calculated FTIR spectra for configuration (c) of 6.2 *in vacuo.*

Figure 6.40. Experimental ATR-FTIR data for pure 6.1.

Figure 6.41. Experimental ATR-FTIR data for pure 6.2.

Figure 6.42. The minimised conformation of the doubly-deprotonated forms (a) to (c) of 6.2.

Figure 6.43. Calculated vibrational data for the doubly-deprotonated form of 6.2.

Figure 6.44. Calculated FTIR spectra of the doubly-deprotonated form of 6.2 *in vacuo*.

Figure 6.45. ATR-FTIR spectra of pure 6.1 and the acid adsorbed onto native sol-gel titania in a 29 : 1 mole ratio of dye to 2 nm titania particles.

Figure 6.46. An expansion of Figure 6.43, of pure 6.1 and the acid adsorbed onto native sol-gel titania in a 29 : 1 mole ratio of dye to 2 nm titania particles.

Figure 6.47. Experimental ATR-FTIR data for pure 6.2 and the dye adsorbed onto sol-gel titania in a 15 : 1 mole ratio of dye to 2 nm titania particles.

Figure 6.48. ATR-FTIR spectrum of pure 6.3 and upon sol-gel titania in an 18 : 1 mole ratio of dye to titania 2 nm in diameter.

Figure 6.49. ATR-FTIR spectra of pure 6.4 and the acid bound to sol-gel titania in an 18 : 1 and in a 21 : 1 mole ratio of dye to titania 2 nm in diameter.

Section 6.5.4.

Figure 6.50. Fluorescence of 6.4 in methanol and with a calculated mole ratio of dye to titania 2 nm in diameter of 39 : 1, 20 : 1, 10 : 1 and 1 : 1. The excitation wavelength was 455 nm.

Figure 6.51. Fluorescence maximum of 6.4 in methanol versus the mole ratio of dye to titania particles 2 nm in diameter. The fluorescence maximum of pure 6.4 is 592 nm. The excitation wavelength was 455 nm. The error bars are for an uncertainty of ± 0.5 nm of the fluorescence signal and approximately ± 7 % for the mole ratio of dye to 2 nm diameter titania.

Figure 6.52. Raman spectra of a methanolic solution with a 12 : 1, a 6 : 1, a 4 : 1 and a 1 : 3 mole ratio of acidic, amorphous 2 nm sol-gel titania to dye 6.4. The non-linear background has not been subtracted.

Section 6.5.5.2.

Figure 6.53. ^{1}H-NMR spectrum of 6.1 in CD_3OD.

Figure 6.54. ^{1}H-NMR spectrum of 6.2 in CD_3OD.
Figure 6.55. ^{1}H-NMR spectrum of 6.4 in CD_3OD.
Figure 6.56. ^{1}H-NMR spectrum of the tetramethylammonium salt of 6.1 in CD_3OD. Pure 6.1, a 1 : 1 mole ratio and a 2 : 1 mole ratio of 6.1 to tetramethylammonium hydroxide.
Figure 6.57. ^{1}H-NMR spectra of a 12 M solution of 6.2 in CD_3OD, titrated with hydrochloric acid. A mole ratio of dye to hydrochloric acid of 1 : 0, 1 : 45, 1 : 89 and 1 : 116.
Figure 6.58. ^{1}H-NMR spectra of 6.3 in CD_3OD, with a mole ratio of dye to hydrochloric acid of 1 : 124 and with a mole ratio of dye to titania particles 2 nm in diameter of 19 : 1.

Section 6.5.5.3.
Figure 6.59. A cartoon of the solvent partition method. a) Sol-gel titania solvated in D_2O is added to a saturated solution of dye in $CDCl_3$. b) Dye diffuses through the solvent-solvent interface and binds to titania in the D_2O layer. c) The D_2O layer was removed by pipette for analysis by NMR spectroscopy.
Figure 6.60. ^{1}H-NMR spectra of the titration of 6.1 with acidic, amorphous, sol-gel titania in CD_3OD. An 8 : 1, 12 : 1 and a 17 : 1 mole ratio of 6.1 to titania particles 2 nm in diameter.
Figure 6.61. ^{1}H-NMR spectrum of the methanol-soluble portion of a titania resuspension experiment. The mole ratio of 6.1 to 2 nm titania particles was 18 : 1. A crude indication of the position of sharp overlaid signals due to free dye.
Figure 6.62. ^{1}H-NMR spectrum of a 2 mM solution of 6.1 in D_2O-DSS.
Figure 6.63. Representations of: (a) the *cis*- and (b) the *trans*- mono-salt forms and (c) the di-salt of 6.1.
Figure 6.64. ^{1}H-NMR spectrum of a saturated solution of 6.1 in D_2O.
Figure 6.65. ^{1}H-NMR spectrum of an initial 12 : 1 mole ratio of 6.1 to 2 nm titania particles in D_2O-DSS.
Figure 6.66. ^{1}H-NMR spectrum of the D_2O layer of a partition experiment that used an initial 17 : 1 mole ratio of 6.1 to 2 nm titania particles.
Figure 6.67. ^{1}H-NMR spectra of the D_2O layer of a solvent partition experiment which used an initial 12 : 1 mole ratio of 6.1 to 2 nm titania particles. A 3x and a 10x dilution in CD_3OD.
Equation 6.3. The Einstein-Stokes equation, using methanol at 298K.

Section 8.1.
Table 8.1. Analysis of the TiO_2, water, solvent and acid content of sol-gel titania.

Section 8.2.
Table 8.2. Experimental extinction coefficients of probe dyes in tetrahydrofuran.
Table 8.3. Theoretical ratios of dye to titania, using estimated surface area for non-sintered native sol-gel titania 2 nm in diameter, with a surface area of 12.57 nm^2 per particle and a molar mass of 10847 g mol^{-1}.
Table 8.4. Theoretical ratios of dye to titania, using estimated surface area for non-sintered native sol-gel titania 3 nm in diameter, with a surface area of 28.27 nm^2 per particle and a molar mass of 36607 g mol^{-1}.

Table 8.5. Theoretical ratios of dye to titania, using estimated surface area for non-sintered native sol-gel titania 4 nm in diameter, with a surface area of 50.27 nm^2 per particle and a molar mass of 86771 g mol^{-1}.

Table 8.6. The amount of dye required for monolayer coverage of sintered Dyesol titania, using the footprint areas shown in Table 8.3.

Table 8.7. The amount of dye required for monolayer coverage of sintered sol-gel titania, using the footprint areas shown in Table 8.3.

Table 8.8. If the surface area of sintered 'native' sol-gel titania is 187 m^2 g^{-1}, if the footprint area of 6.1 is 4.5 x 10^{-19}, a monolayer dye loading is 6.9 x 10^{-4} mol g^{-1}. Supposing that the sintered material was still composed of discrete spheres, then the mole ratio between dye and titania spheres is given by n(dye) : n(TiO_2). The percentage dye loading of sintered titania over that of native sol-gel titania gives an indication of the degree of particle aggregation introduced by sintering.

Table 8.9. UV-Vis absorption of dyes on sintered titania.

Figure 8.1. The integrated area of the UV-Vis absorption of sintered Dyesol titania dyed with 6.5. The red shift in dye absorbance is due to rearrangement of dye on titania due to the loss of solvent, rather than to a decrease in the amount of dye present. The integrated region was 390 to 700 nm. Data is shown for samples immersed in a 0.2 mM solution of 6.5 in tetrahydrofuran for: a) 3 minutes, wet and dried; b) 6 minutes, wet and dried.

Figure 8.2. The fluorescence intensity of 6.4, in methanol, normalised to absorbance. Two sets of data are displayed. The error bars are for conservative uncertainties of ± 50 counts of intensity and ± 10% of concentration.

ABBREVIATIONS

AFM	Atomic force microscopy, a type of scanning probe microscopy.
AM 1.5	Air mass 1.5. 'One Sun'. Equivalent to 100 mW cm^{-2}, the intensity of solar light when the sun is 48.2° from zenith.[1-3]
ATR-FTIR	Attenuated total internal reflectance Fourier transform infra-red spectroscopy.
CVD	Chemical vapour deposition.
DSSC	Dye-sensitised solar cell; Grätzel cell..
ITO	Indium-doped tin oxide. Commonly used to coat glass for a conductive surface.
SEM	Scanning electron microscopy.
SPM	Scanning probe microscopy.
STM	Scanning tunnelling microscopy, which is a type of scanning probe microscopy.
TEM	Transmission electron microscopy.
UV-Vis	Ultra-violet and visible light.
XRD	X-ray diffraction

DEFINITIONS AND SYNONYMS

Aqua Regia
1 : 3 v/v concentrated (fuming) nitric acid to concentrated (1.18 g mL^{-1}) hydrochloric acid. If the solution is to be stored, include 1 volume of water.[4]

Bohr radius
The Bohr radius is unique for each substance and is the distance between the electron and hole of a Mott-Wannier pair, or 'exciton'.

Dyesol Limited
Previously known as Sustainable Technologies Australia (STA), then as Sustainable Technologies International Pty Ltd (STI).

External Quantum Efficiency (EQE)
Of a solar cell: also known as the incident photon conversion efficiency, which is the number of electrons generated per incident photon.[5] $EQE = n_e/n_{hv} = (I_{sc}.hc)/(P_o.\lambda_e)$

Fill-Factor (ff)
Of a solar cell: the maximum electrical power generated divided by the product of the short-circuit current and the open circuit voltage. The maximum power generated is the product of the short circuit current (maximum) and the open circuit voltage (maximum). $ff = (I_{max}.V_{max})/(I_{sc}.V_{oc})$

Global conversion efficiency (η_{global})
Of a solar cell: the maximum electrical power generated divided by the intensity of the incident light. $\eta_{global} = (I_{max}.V_{max})/I_s$

Grätzel Cell
A liquid heterojunction DSSC which employs a mesoporous and nanocrystalline titania electrode that has been sensitised to absorb visible light.

Inverse Opal
Inverse colloidal crystal, reverse-contrast colloidal crystal, air-sphere colloidal crystal.

Macrostructure
A structure with dimensions larger than 100 nm.

Nanocrystalline
A material that is crystalline with dimensions on the order of nanometres. The term is often used in reference to particulate material which may be composed of smaller particles.

Nanoparticles
Particles with a size on the order of nanometres.

Nanostructure
The structuring of materials such that at least one dimension that is less than a hundred nanometres wide.

Opal
A colloidal crystal. Specifically, opal refers to a colloidal crystal of silica.

Polydispersity Index
Equals the weight-average molecular weight divided by the number-average molecular weight. The number-average is never greater than the weight-average and the larger the index, the wider is the distribution.

Power Conversion Efficiency (η_{eff})
Of solar cells: the maximum electrical power generated divided by the incident optical power. $\eta_{eff} = (I_{max}.V_{max})/P_o$

Polyelectrolyte
A polymer in which the degree of ionisation is dependent on the pH of the environment.[6]

Piranha Solution
Either a 2 : 1 v/v, a 3 : 1 v/v or a 4 : 1 solution of concentrated (96%) sulfuric acid to 30% aqueous hydrogen peroxide.[7-9]

Quantum dot
A material that is quantum-confined in three-dimensions.

Relative Centrifugal Force (rcf)
Calculated from the rotations per minute (rpm) and the swing radius of the centrifuge. The units of measure are 'g', for gravitational acceleration.

Root Mean Square (RMS)
Quadratic mean. $RMS = ((\Sigma x_i)^2)/n)^{1/2}$

Screen-printing
Equivalent to tape-casting of material by pressing material through a mesh screen. The paste viscosity, mesh size, thread thickness and the tension of the screen determine the film thickness.

Sol; Sol-gel
A suspension of tiny particles, which may be stabilised; a gel formed of a sol.

Superlattice
An arrangement of material which recalls the ordering found within ionic lattices.

Tape-casting
Doctor-blading, where a film is cast onto a substrate by application of a blade along guide rails or a mask. The paste viscosity and the height of the mask or guide determines the film thickness.

$V_{Ag/Ag+}$
Potential with respect to a psuedo-reference electrode of silver/silver ion.

V_{SCE}
Potential with respect to a standard calomel electrode.

References

1. Green, M A; Emery, K; King, D L; Igari, S; Warta, W. Solar Cell Efficiency Tables (Version 24). *Progress in Photovoltaics: Research and Applications* **2004**, 12, 365-372.

2. Sun, S-S; Sacriciftci, N S. *Organic Photovoltaics. Mechanisms, Materials and Devices*. Taylor & Francis Group, Florida, USA: **2005**.

3. Grätzel, M. Mesoscopic Solar Cells for Electricity and Hydrogen Production from Sunlight. *Chemistry Letters* **2005**, 34, 8-13.

4. Weast, R C; Lide, D R; Astle, M J; Beyer, W H. *CRC Handbook of Chemistry and Physics*. 70th ed, CRC Press Inc.: Boca Raton, Florida, **1989**.

5. Sun, S-S; Sariciftci, N S. *Organic Photovoltaics: Mechnisms, Materials and Devices*. Taylor & Francis Group: Florida, USA, **2005**.

6. Yap, H P; Quinn, J F; Ng, S M; Cho, J; Caruso, F. Colloid Surface Engineering via Deposition of Multilayered Thin Films from Polyelectrolyte Blend Solutions. *Langmuir* **2005**, 21, 4328-4333.

7. Wang, M; Leichti, K M; Wang, Q; White, J M. Self-Assembled Silane Monolayers: Fabrication with Monoscale Uniformity. *Langmuir* **2005**, 21, 1848-1857.

8. Bocking, T; Salomon, A; Cahen, D; Gooding, J J. Thiol-Terminated Monolayers on Oxide-Free Si: Assembly of Semiconductor-Alkyl-S-Metal Junctions. *Langmuir* **2007**, 23, 3236-3241.

9. Armstrong, N R; Carter, C; Donley, C; Simmonds, A; Lee, P; Brumbach, M; Kippelen, B; Domercq, B; Yoo, S. Interface Modification of ITO Thin Films: Organic Photovoltaic Cells. *Thin Solid Films* **2003**, 445, 342-352.

PICTORIAL TABLES OF ORGANIC SPECIES

Ferrocenyl compounds for the functionalisation of ITO

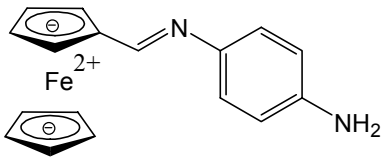	*Compound* ***5.3*** *N*-(ferrocenylmethylidene)-4-phenylenediamine *N*-(ferrocenylmethylidene)-*p*-phenylenediamine Mono-Schiff Base. 304 g mol^{-1}. *Synthesised by Ms. Yvonne Ting*
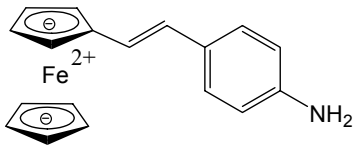	*Compound* **5.4** 2-(4-aminophenyl)ethenylferrocence 2-(*p*-aminophenyl)ethenylferrocence RJD-99-3. 303 g mol^{-1}. *Synthesised by Mr. Ross Davidson.*
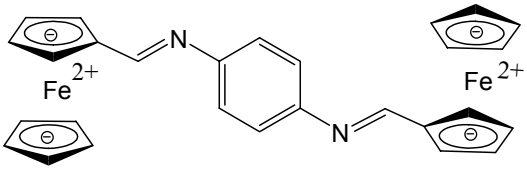	*N,N'*-di(ferrocenylmethylidene)-4-phenylenediamine *N,N'*-di(ferrocenylmethylidene)-*p*-phenylenediamine Di-Schiff Base. 500 g mol^{-1}. Synthesised by Ms. Yvonne Ting.

Small organic dyes for binding to titania

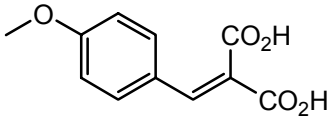	Compound **6.1** 4-methoxybenzylidenemalonic acid 4-methoxyphenylmethylene propanedioic acid *p*-methoxybenzylidene malonic acid *p*-methoxybenzal malonic acid 060720. 222 g mol^{-1}. *Synthesised by Ms. Yvonne Ting.*
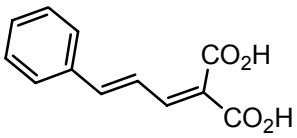	Compound **6.2** Cinnamylidenemalonic acid. (3-phenyl-2-propenylidene)-propanedioic acid 3-phenyl-2-propenylidene propanedioic acid AWIS-126. 218 g mol^{-1}. *Synthesised by Mr. Adam Stephenson.*

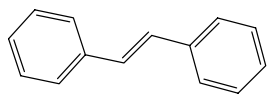	*Trans*-stilbene. *Trans*-1,2-diphenyl-1-ethene 180 g mol^{-1}.

Ter(thienylenevinylene) and ter(thienylvinylene) dyes for binding to titania

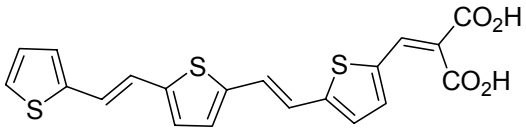	Compound **6.3** Ter(thienylenevinylene)malonic acid Ter(thiophene-2,5-diyl)vinylenemalonic acid (*E,E*)-(2-(5-(2-(5-(2-(2-thienyl)vinyl)-2-thienyl)vinyl)thiophenevinylmalonic acid 5-((5-(2-thien-2-ylethenyl)thien-2-ylethenyl)thien-2yl malonic acid E-491. 414.5 g mol^{-1}. Synthesised by Dr. Pawel Wagner.
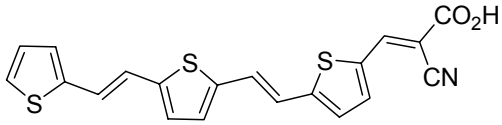	Compound **6.4** Ter(thienylenevinylene)cyanoacetic acid 2-cyano-3[2,2',5',2"]terthiophen-5-yl acrylic acid 5-((5-(2-thien-2-ylethenyl)thien-2-ylethenyl)thien-2yl cyanoacetic acid E-490. 395.5 g mol^{-1}. Synthesised by Dr. Pawel Wagner.
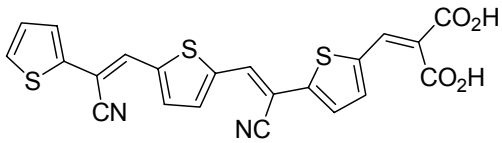	Compound **6.5** 8,15-dicyanoter(thienylenevinylene)-malonic acid 2-(5-(1-cyano-2-(5-(2(thiophen-2-yl)ethenyl)thiophen-2-yl)ethenyl)-thiophen-2-ylmethylene)malonic acid E-513. 464.5 g mol^{-1}. Synthesised by Dr. Pawel Wagner.
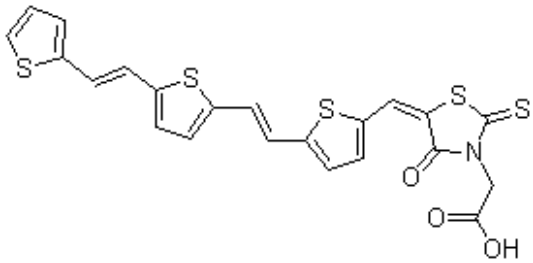	Compound **6.6** Ter(thienylenevinylene)rhodanine acetic acid EM-59. 503 g mol^{-1}. Synthesised by Dr. Pawel Wagner.

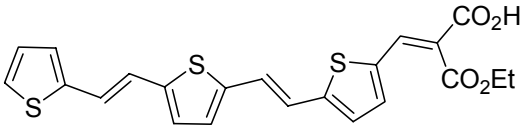	Ter(thienylenevinylene)malonate monoethyl ester EM-50. 442.5 g mol^{-1}. Synthesised by Dr. Pawel Wagner.
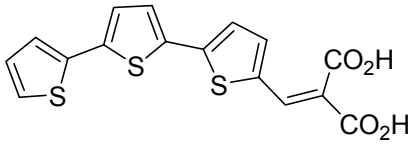	Terthienylvinylenemalonic acid 3-((2,2':5',2")terthiophen-5-yl)malonic acid SG-72/5. 362.4 g mol^{-1}. Synthesised by Dr. Sanjeev Ghambir.
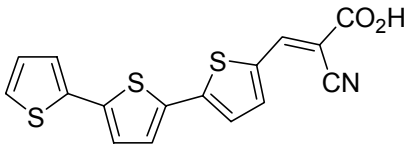	Terthienylcyanoacrylic acid 2-cyano-3-((2,2':5',2")terthiophen-5-yl)acrylic acid SG-74/5. 343.4 g mol^{-1}. Synthesised by Dr. Sanjeev Ghambir.

Porphyrin dyes and coordination compounds for binding to titania

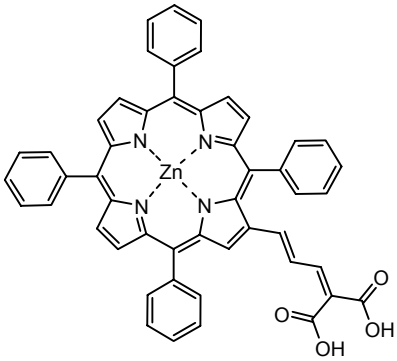	Compound **6.7** 4-(2'-(5',10',15',20'-tetraphenylporphyrinato zinc(II)yl)butadienylmalonic acid 4-(2'-(5',10',15',20'-tetraphenylporphyrinato zinc(II)yl)allylidenemalonic acid WMC-236. Zn-2a. 818.2 g mol^{-1}. Synthesised by Dr. Wayne Campbell.
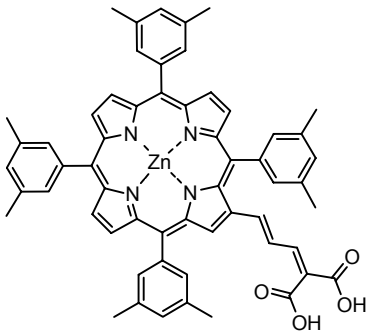	Compound **6.8** 4-(2'-(5',10',15',20'-tetraxylylporphyrinato zinc(II)yl)butadienylmalonic acid 4-(2'-(5',10',15',20'-tetraxylylporphyrinato zinc(II)yl)allylidenemalonic acid WMC-299B. Zn-2g. 930.4 g mol^{-1}. Synthesised by Dr. Wayne Campbell.

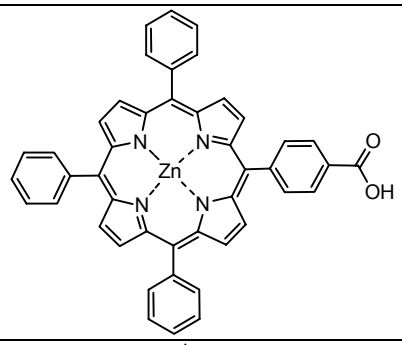	Compound **6.9** (5'-(10',15',20'-triphenylporphyrinato zinc(II))-4-benzoic acid EM-95. 722.12 g mol^{-1}. Synthesised by Dr. Pawel Wagner.
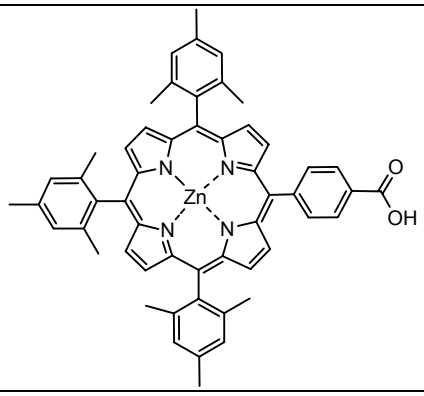	Compound **6.10** (5'-(10',15',20'-trimesitylporphyrinato zinc(II))-4-benzoic acid 5-(4-carboxyphenyl)-10,15,20-trimesitylporphyrinato zinc(II) EM-55. 848.4 g mol^{-1}. Synthesised by Dr. Pawel Wagner.
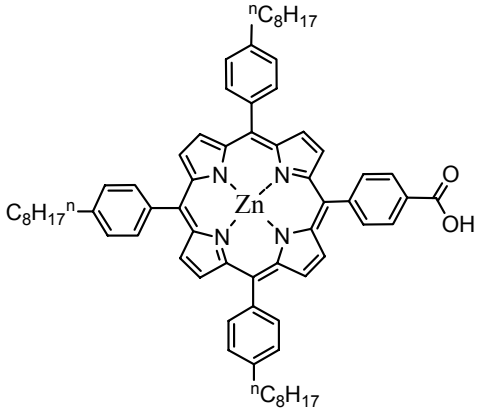	Compound **6.11** (5'-(10',15',20'-tri-(4-*n*-octylphenyl)porphyrinato zinc(II))-4-benzoic acid EM-84. 1058.8 g mol^{-1}. Synthesised by Dr. Pawel Wagner.
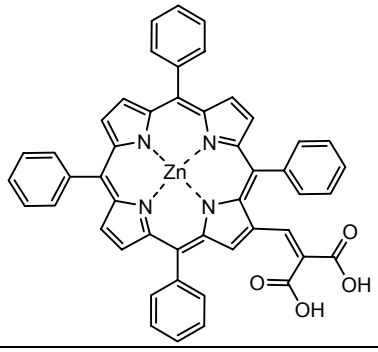	4-(2'-(5',10',15',20'-tetraphenylporphyrinato zinc(II)yl)ethenylmalonic acid WMC-221. Zn-1a. 792.2 g mol^{-1}. Synthesised by Dr. Wayne Campbell.
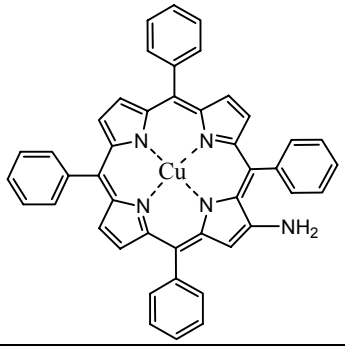	2-(5'-(10',15',20'-tetraphenylporphyrinato zinc(II))-amine EM-428. 690.6 g mol^{-1}. Synthesised by Dr. Pawel Wagner.

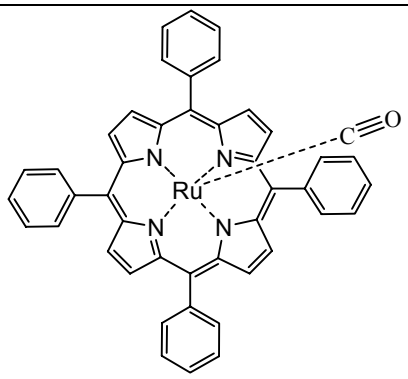	Carbonyl(5’,10’,15’,20’-tetraphenylporphyrinato ruthenium(II) Carbonyl(tetraphenylporphyrinato) ruthenium(II) RuTPPCO. 742.2 g mol^{-1}. Synthesised by Dr. Sanjeev Ghambir.
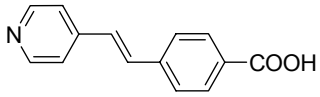	γ-stilbazole-4’-carboxylic acid 4-[*trans*-2-(pyrid-4-yl-vinyl)]-benzoic acid 4-(*trans*-2-(4-pyridinyl)ethenyl)-benzoic acid 060306. 225 g mol^{-1}. Synthesised by Ms. Yvonne Ting.
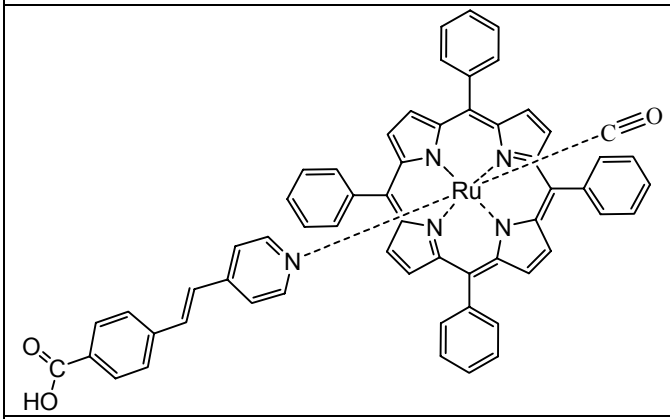	Carbonyl(5’,10’,15’,20’-tetraphenylporphyrinato ruthenium(II) with 4-(*trans*-2-(4-pyridinyl)ethenyl)benzoic acid. 060327. 967 g mol^{-1}. Synthesised by Ms. Yvonne Ting.
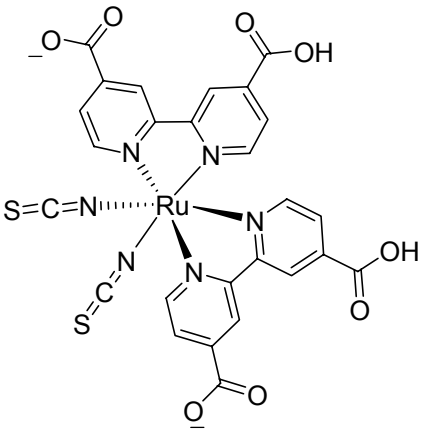	*Cis*-bis(isothiocyanato)bis(2,2'-bipyridyl-4,4'-dicarboxylato)-ruthenium(II) bis-tetrabutylammonium Ru ‘N3’ dye, Ru-535 bis-TBA, DyeSol B2/N719. 1188.5 g mol^{-1}. 1260.5 g mol^{-1} with $4H_2O$. Purchased from DyeSol, Australia.